World Journal of Radiology

Online Submissions: http://www.wjgnet.com/esps/
wjr@wjgnet.com
doi:10.4329/wjr.v5.i5.202

World J Radiol 2013 May 28; 5(5): 202-207
ISSN 1949-8470 (online)

BRIEF ARTICLE

Correlation analysis of dual-energy CT iodine maps with quantitative pulmonary perfusion MRI

Jan Hansmann, Paul Apfaltrer, Frank G Zoellner, Thomas Henzler, Mathias Meyer, Gerald Weisser, Stefan O Schoenberg, Ulrike I Attenberger

Jan Hansmann, Paul Apfaltrer, Thomas Henzler, Mathias Meyer, Gerald Weisser, Stefan O Schoenberg, Ulrike I Attenberger, Institute of Clinical Radiology and Nuclear Medicine, University Medical Center Mannheim, Medical Faculty Mannheim, Heidelberg University, D-68167 Mannheim, Germany
Frank G Zoellner, Computer Assisted Clinical Medicine, Medical Faculty Mannheim, Heidelberg University, D-68167 Mannheim, Germany
Author contributions: All authors made substantial contributions to the conception and design of the study, drafting or revising the article critically for important intellectual content; Hansmann J, Apfaltrer P, Zoellner FG and Attenberger UI contributed to the data analysis and interpretation.
Correspondence to: Jan Hansmann, MD, Institute of Clinical Radiology and Nuclear Medicine, University Medical Center Mannheim, Medical Faculty Mannheim, University of Heidelberg, Theodor-Kutzer-Ufer 1-3, D-68167 Mannheim, Germany. jan.hansmann@medma.uni-heidelberg.de
Telephone: +49-621-3832067 Fax: +49-621-3833817
Received: January 14, 2013 Revised: May 3, 2013
Accepted: May 16, 2013
Published online: May 28, 2013

Abstract

AIM: To correlate dual-energy computed tomography (DECT) pulmonary angiography derived iodine maps with parameter maps of quantitative pulmonary perfusion magnetic resonance imaging (MRI).

METHODS: Eighteen patients with pulmonary perfusion defects detected on DECT derived iodine maps were included in this prospective study and additionally underwent time-resolved contrast-enhanced pulmonary MRI [dynamic contrast enhanced (DCE)-MRI]. DCE-MRI data were quantitatively analyzed using a pixel-by-pixel deconvolution analysis calculating regional pulmonary blood flow (PBF), pulmonary blood volume (PBV) and mean transit time (MTT) in visually normal lung parenchyma and perfusion defects. Perfusion parameters were correlated to mean attenuation values of normal lung and perfusion defects on DECT iodine maps. Two readers rated the concordance of perfusion defects in a visual analysis using a 5-point Likert-scale (1 = no correlation, 5 = excellent correlation).

RESULTS: In visually normal pulmonary tissue mean DECT and MRI values were: 22.6 ± 8.3 Hounsfield units (HU); PBF: 58.8 ± 36.0 mL/100 mL per minute; PBV: 16.6 ± 8.5 mL; MTT: 17.1 ± 10.3 s. In areas with restricted perfusion mean DECT and MRI values were: 4.0 ± 3.9 HU; PBF: 10.3 ± 5.5 mL/100 mL per minute, PBV: 5 ± 4 mL, MTT: 21.6 ± 14.0 s. The differences between visually normal parenchyma and areas of restricted perfusion were statistically significant for PBF, PBV and DECT ($P < 0.0001$). No linear correlation was found between MRI perfusion parameters and attenuation values of DECT iodine maps (PBF: $r = 0.35$, $P = 0.15$; PBV: $r = 0.34$, $P = 0.16$; MTT: $r = 0.41$, $P = 0.08$). Visual analysis revealed a moderate correlation between perfusion defects on DECT iodine maps and the parameter maps of DCE-MRI (mean score 3.6, κ 0.45).

CONCLUSION: There is a moderate visual but not statistically significant correlation between DECT iodine maps and perfusion parameter maps of DCE-MRI.

Key words: Dual-energy computed tomography; Time-resolved magnetic resonance imaging; Pulmonary perfusion; Iodine maps

Core tip: Dual-energy derived iodine maps and dynamic contrast enhanced magnetic resonance imaging (DCE-MRI) may allow evaluation of pulmonary perfusion. Hypothetical the decrease in pulmonary perfusion detected on DCE-derived iodine maps would correlate highly with perfusion parameters derived from DCE-MRI in patients with restricted pulmonary perfusion.

However, against our hypothesis, we did not find a significant correlation between pulmonary perfusion defects detected on dual-energy computed tomography-derived iodine maps and perfusion parameters derived from time-resolved MRI. In addition, there was only a moderate level of visual correlation. This is in contrast with prior studies that investigated the role of pulmonary iodine maps to serve as an additional tool providing a functional evaluation of pulmonary perfusion.

Hansmann J, Apfaltrer P, Zoellner FG, Henzler T, Meyer M, Weisser G, Schoenberg SO, Attenberger UI. Correlation analysis of dual-energy CT iodine maps with quantitative pulmonary perfusion MRI. *World J Radiol* 2013; 5(5): 202-207 Available from: URL: http://www.wjgnet.com/1949-8470/full/v5/i5/202.htm DOI: http://dx.doi.org/10.4329/wjr.v5.i5.202

INTRODUCTION

Dual-energy computed tomography (DECT) was first introduced in the late 1970s and allows for the differentiation of materials based on their X-ray attenuation at different tube voltages[1]. Different vendors have reintroduced DECT and in recent years the technique has become clinically feasible[2,3]. DECT has been investigated for a variety of organ systems[4-8], however, pulmonary imaging and in particular dual-energy derived iodine maps have been the focus of multiple previous studies[9-12]. Dual-energy derived iodine maps allow the visualization of parenchymal iodine distribution in relation to a previously defined scan delay, which might be considered as a surrogate of pulmonary perfusion and has shown good correlation compared to nuclear medicine based imaging modalities[9,10,13]. Another modality that allows an evaluation of pulmonary perfusion disorders is dynamic contrast enhanced magnetic resonance imaging (DCE-MRI)[14-17]. Multiple pulmonary perfusion parameters can be derived from DCE-MRI by means of post-processing, including pulmonary blood flow (PBF), pulmonary blood volume (PBV) and mean transit time (MTT). To our knowledge, no prior study correlated the perfusion changes shown in time resolved perfusion imaging modalities such as DCE-MRI to the perfusion changes displayed in DECT-derived iodine maps. We hypothesized that a decrease in pulmonary perfusion detected on DECT-derived iodine maps would correlate highly with perfusion parameters derived from DCE-MRI in patients with restricted pulmonary perfusion regardless of the underlying cause of pulmonary perfusion restriction.

MATERIALS AND METHODS

Patients

This monocentric, prospective, non-randomized study was approved by our institutional review board. The nature of our study was explained entirely to all patients prior to enrollment and written informed consent was obtained from all participants. Eighteen consecutive patients (11 men and 7 women, mean age 61 years, range 20-81 years) were prospectively enrolled in our study. The inclusion criterion was a perfusion defect detected on iodine maps derived from DECT pulmonary angiography (DE-CTPA). Exclusion criteria were renal insufficiency defined as a serum creatinine level > 1.5 mg/d, hemodynamic instability or general contraindications to MRI. Pulmonary perfusion deficits were due to a number of underlying pathology, including pulmonary embolism (n = 8), severe emphysema (n = 5) and postobstructive perfusion defects due to lung cancer (n = 5).

Dual energy computed tomography

All examinations were performed on a 64-channel first generation dual-source computed tomography (CT) scanner (Somatom Definition, Siemens Health Care, Forchheim, Germany). The system is equipped with two X-ray tubes and two corresponding detectors mounted in a 90 degree angle to each other in the gantry. One detector array (corresponding to tube A) provides a field of view of 50 cm, while the other detector array (corresponding to tube B) is limited to field of view of 26 cm. Tube voltages for tube A were set to 140 kV and to 80 kV for tube B. To compensate for the lower photon output of tube B, the quality reference tube current was set to 235 mAs for tube B and 50 mAs for tube A. Tube rotation time was 0.33 s. Automatic tube current modulation (CARE Dose 4D, Siemens Health Care Sector, Forchheim, Germany) was used in all patients. According to the manufacturer's recommendations, the detector collimation was set to 14 mm × 1.2 mm to minimize beam-hardening artefacts and improve signal-to-noise ratio. A separate dataset for each tube kV as well as a linearly weighted average dataset ("virtual 120 kV", using 70% tube A and 30% tube B) was calculated with a slice thickness of 2 mm and a reconstruction increment of 1.5 mm using a soft tissue kernel (D30f). All scans were performed in caudocranial direction during a midinspiratory breath-hold.

Contrast material was injected using 18 or 20 G intravenous catheters placed in the left or right antecubital vein using an automated power injector (Stellant D CT Injection System MEDRAD Inc, Warrendale, PA) and utilizing a bolus tracking technique, in which the scan was started with a 10 s delay after a threshold of 100 Hounsfield units (HU) was reached in the pulmonary trunk. Injection rate was 3.5 mL/s. All contrast injections were followed by an additional saline (NaCl) flush of 50 mL, injected at the same rate used for the previous contrast agent injection.

MRI

All pulmonary time resolved magnetic resonance angiography (MRA) exams were performed on a 3.0 Tesla 128 channel MR system (Magnetom Skyra, Siemens AG, Healthcare Sector, Erlangen, Germany). For signal reception, a body matrix coil with 18 elements as well as 18 elements of the inbuilt spine matrix were used. First, 2D gradient echo localizers and a coronal T_2-weighted

half acquisition turbo spin echo sequence were applied to ensure correct preparation of the MRA exam. Time resolved MRA was applied using a 3D time resolved angiography with interleaved stochastic trajectories pulse sequence, which combines parallel imaging with view-sharing to decrease the acquisition time. In detail, the following imaging parameters were used: echo time = 0.8 ms, repetition time = 2.2 ms, bandwidth = 815 Mhz/px, generalized autocalibrating partially parallel acquisition = 2, field of view = 375 × 500, voxel size = 2.0 × 2.0 × 5.0 mm^3, acquisition time was 58 s. Patients were asked to hold their breath in mid inspiratory breathhold as long as possible and to continue shallow breathing until completion of the sequence. Eighteen or 20 G access was obtained in the left or right antecubital fossa. An automated power injector (Medrad Spectris Solaris EP, Medrad Indianola, PA) was used for the injection of the contrast agent. A dose of 0.07 mmol/kg per body weight of gadoterate meglumine (Dotarem, Guerbet, France) was used. The injection rate of the contrast material was 3.0 mL/s followed by a 20 mL chaser of saline (NaCl), injected at the same rate.

Data analysis

Iodine maps were generated on a commercially available workstation (Leonardo, Siemens Healthcare) using the commercially available Syngo Pulmonary Blood Volume software (Syngo VA 21, Siemens Health Care Sector, Forchheim, Germany). After loading both 80-kV and 140-kV images into the software, the iodine content of each voxel is derived through a three-material-decomposition algorithm for air, soft tissue, and iodine. Multiplanar reformations for iodine maps were generated using a slice thickness of 2 mm, with a 1.5 mm increment.

MRA data were quantitatively analyzed using a pixel-by-pixel deconvolution analysis using an in-house developed software plugin, integrated into a standard digital imaging and communications in medicine viewer (the OsiriX Foundation, Geneva, Switzerland). The underlying algorithm is a modification of the highly successful truncated singular value decomposition algorithm with a fixed regularization parameter, as first proposed for DCE-MRI by Ostergaard *et al*[18]. To allow for perfusion analysis of T1-weighted DCE-MRI, the conversion of signal to concentration is modified and the convolution product is discretised using the Volterra formula as proposed by Sourbron *et al*[19,20]. Using an in-house test suite of artificial data demonstrated that the plug-in can produce similar values as a published and widely used reference implementation in PMI 0.4[19,20]. Here, on average the difference on pixel basis for the parameters plasma flow (in units of mL/100 mL per minute), volume of distribution (in units of mL/100 mL), and MTT (in units of second) was less than 0.05.

Image evaluation

Parenchymal attenuation was measured in perfusion defects and visually normal parenchyma on DECT-derived iodine maps using the previously described Pulmonary Blood Volume software (Syngo VA 21, Siemens Health Care Sector, Forchheim, Germany). Three region of interests (ROIs) were placed on consecutive slices in areas of restricted perfusion. Three ROIs were placed on consecutive slices in visually normal parenchyma of the same lung (*i.e.*, right or left). Care was taken to exclude pulmonary vessels in order to avoid artifacts. The mean "overlay value" of the ROIs was noted which represents the pure dual-energy calculated iodine distribution within the parenchyma. The mean value as well as the standard deviation of the three measurements were calculated. ROI size was not standardized between patients due to the different size of perfusion defects encountered but was identical between areas of restricted perfusion and normal parenchyma.

ROIs corresponding to the location of the ROIs placed for DECT iodine maps were placed in the areas of restricted perfusion as well as normal parenchyma on MRI parameter maps. Again, three consecutive slices were chosen and the mean regional PBF, PBV and MTT were averaged from the ROI measurements. Perfusion parameters were correlated to mean attenuation values measured in perfusion defects and normal parenchyma in DECT-derived iodine maps using Pearsons's correlation analysis.

In addition, two readers both with more than 10 years of experience in thoracic imaging rated the correlation of perfusion defects between the two modalities in a visual analysis using a 5-point Likert scale (1 = no correlation, 2 = poor correlation, 3 = fair correlation, 4 = good correlation, 5 = excellent correlation). The correlation between modalities was first assessed by each reader individually before a consensus was established for each patient. Readers were blinded to the patients' history and diagnosis. Figure 1 provides an example of the perfusion deficits observed in this study. Inter-reader correlation was assessed using kappa statistics.

Statistical analysis

Statistical analysis was performed using JMP 9.0 (SAS Institute, Cary, NC, United States). Continuous variables are expressed as mean ± SD. The Shapiro-Wilk test was applied to determine probability distribution; a two-tailed Student's *t*-test was subsequently used to compare groups with normal distribution, while the Mann-Whitney-*U*-test was used if the data were not normally distributed. The χ^2 test was applied for dichotomous variables. Pearson's correlation was used to correlate perfusion defects detected on DECT-derived iodine maps with to the corresponding PBF, PBV and MTT. A 2-tailed *P*-value of < 0.05 was considered statistically significant.

RESULTS

Mean time delay between DECT and DCE-MRI was 2.6 d (range 0-12 d). In acute pulmonary perfusion disorders (*e.g.*, pulmonary embolism) the mean time between examinations was 22 h (range 4-48 h). In 14 of 18 patients undergoing DECT up to 3.4 cm of the peripheral lung

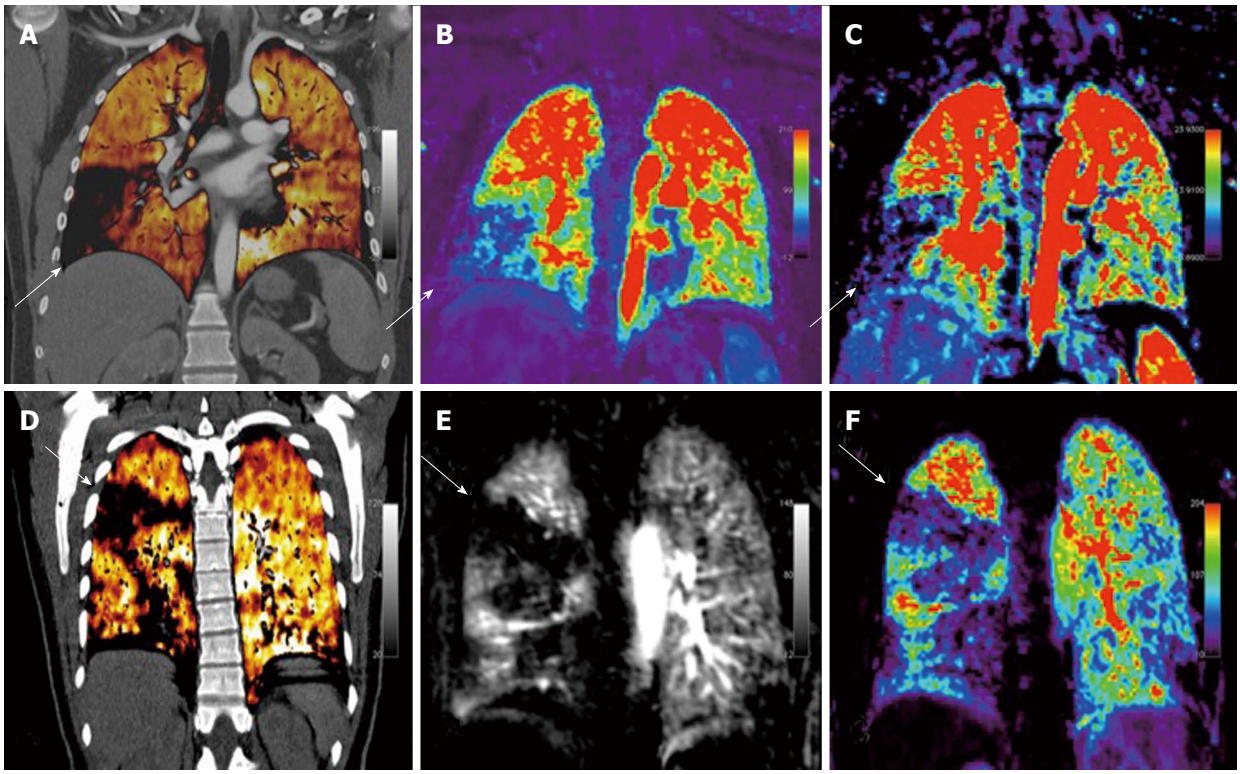

Figure 1 Correlation of perfusion deficits in a 20-year-old male and 42-year-old female male with pulmonary embolism (arrows pointing to perfusion defects). A, D: Dual-energy computed tomography derived iodine map; B, E: Pulmonary blood flow; C, F: Pulmonary blood volume.

Table 1 Mean dynamic contrast enhanced-magnetic resonance imaging and dual-energy computed tomography values and SD in visually normal pulmonary parenchyma and areas with restricted perfusion

	Visually normal parenchyma	Perfusion defect	*P* value
PBF (mL/100 mL per minute)	58.8 ± 36	10.3 ± 5.5	< 0.0001
PBV (mL)	16.6 ± 8.5	5.0 ± 4.0	< 0.0001
MTT (s)	17.1 ± 10.3	21.6 ± 14	0.28
Lodine map (HU)	22.6 ± 8.3	4.0 ± 3.9	< 0.0001

The attenuation given for the Iodine Map represents the pure dual-energy calculated iodine distribution within the pulmonary parenchyma. PBF: Pulmonary blood flow; PBV: Pulmonary blood volume; MTT: Mean transit time; HU: Hounsfield units.

parenchyma was not covered due to the reduced field of view of the second detector of the first generation dual-source CT, thus not allowing for perfusion analysis in these areas.

Mean attenuation values in DE derived iodine maps were significantly lower in perfusion defects compared to normal parenchyma [4 HU (SD ± 3.9) *vs* 22.6 HU (SD ± 8.3), $P < 0.0001$]. The mean values of the quantitative perfusion parameters in the correlating perfusion defects detected on DCE-MRA were 10.3 mL/100 mL per minute (SD ± 5.5) for PBF, 5 mL (SD ± 4) for PBV and 21.6 s (SD ± 14) for MTT. In visually normal pulmonary tissue mean PBF values were 58.8 mL/ 100 mL per minute (SD ± 36), mean PBV was 16.6 mL (SD ± 8.5) and mean MTT was 17.1 s (SD ± 10.3). Statistically significant differences were observed between PBF and PBV measurements in perfusion defects compared to healthy pulmonary parenchyma with a *P* value of < 0.0001. No statistically significant difference was found for MTT measured in perfusion defects compared to healthy pulmonary parenchyma ($P = 0.28$). Table 1 summarizes the findings.

Pearson correlation showed no correlation between perfusion defects measured on DECT-derived iodine maps and PBF, PBV or MTT measured in the corresponding perfusion defects on DCE-MRI (PBF: $r = 0.35$, $P = 0.15$; PBV: $r = 0.34$, $P = 0.16$; MTT: $r = 0.41$, $P = 0.08$).

The visual analysis showed a moderate correlation between the two modalities, with a median score of 3.8 (SD ± 0.8) for reader 1 and 3.6 (SD ± 0.9) for reader 2. The consensus read revealed a median score of 3.6 (SD ± 0.9) for both readers. Interreader agreement was moderate with a kappa of 0.45 ($P = 0.02$).

DISCUSSION

Our results did not show a significant correlation between pulmonary perfusion defects detected on DECT-derived iodine maps and perfusion parameters derived from time-resolved MRI. In addition, there was only a moderate level of visual correlation. This is in contrast with prior studies that investigated the role of pulmonary iodine maps to serve as an additional tool providing a functional evaluation of pulmonary perfusion. Thieme *et al*[9,10] found a sensitivity/specificity of 100% and 100% of DE-CTPA for the diagnosis of acute pulmonary per-

fusion deficits compared to SPECT/CT and a per segment sensitivity/specificity of 83%/99% with a negative predictive value of 93% for DECT when correlated with pulmonary scintigraphy. In acute pulmonary perfusion disorders such as pulmonary embolism, perfusion defects detected on iodine maps have shown good correlation with morphologic CTPA data[13,21-26]. In pulmonary embolism iodine maps add a further diagnostic criterion whether or not a perfusion defect is present, since small subsegmental pulmonary emboli are sometimes challenging to detect on standard CTPA-images. Perfusion defects caused by these small emboli can be detected on iodine maps, thus possibly raising the detection rate of small, subsegmental pulmonary emboli and at the same time allowing for an assessment of the perfusion deficit associated with the detected embolus. The fact that we did not observe a strong correlation between the two modalities investigated in our study might be related to the broad inclusion criteria for our study since we included patients with a variety of underlying pulmonary pathology including lung cancer, emphysema and acute perfusion disorders such as pulmonary embolism. In addition, only a small number of patients were included in this study, and therefore our results should be viewed as preliminary. Certainly further studies including a larger number of patients and focusing on one disease entity (*e.g.*, pulmonary embolism) seem warranted. Despite the potential advantage of DECT-derived iodine maps, applying them to pulmonary imaging is not without pitfalls. Iodine maps are prone to artifacts due to hyperdense contrast material especially in the inflow tract of the upper thoracic vasculature[12]. Therefore, iodine perfusion maps should not be used as a standalone tool but should only be used in conjunction with standard morphological CTPA data. Generation of iodine maps on a standard workstation is not a time consuming task and can be easily integrated alongside standard reconstructions already used in a routine setting. Radiation dose for DECT has been reported to be within the range of 2-6 mSv and is thus comparable to standard MDCT.

Limitations

Several limitations exist for our study: As this was an initial study only a small sample size of 18 patients was included. A well known limitation of first-generation DE scanners is the 26 cm detector width of the second detector, thus not allowing for the lung periphery in larger patients to be included in the calculations of iodine maps. This problem has been addressed with second-generation scanners. Dual-energy derived iodine maps are prone to artifacts due to beam-hardening from hyperdense contrast material especially in the superior vena cava and the right heart. Nance *et al*[12] found these artifacts to be present in 97% of iodine maps in of a sample of 100 patients. These artifacts have the potential to obscure true perfusion defects or to cause false-positive results. This prevents iodine maps from being used as the sole means to detect pulmonary perfusion disorders and make it mandatory to correlate findings to standard CTPA images. There was a time delay between image acquisition in both modalities, however, in acute pulmonary perfusion disorders such as pulmonary embolism the mean time between DECT and MRI was 24 h with a maximum delay of 48 h in one patient.

Our findings show that perfusion deficits detected on static dual-energy derived iodine maps show a moderate visual correlation with time-resolved DCE-MRI, thus allowing for an assessment of pulmonary perfusion changes as related to a variety of pathology. However, there was no statistically significant correlation between the two modalities, and therefore a prospective study focusing on one entity of pulmonary perfusion disorders (*e.g.*, pulmonary embolism) seems warranted.

COMMENTS

Background

Both, dual-energy computed tomography (DECT) and dynamic contrast enhanced magnetic resonance imaging (DCE-MRI) have been applied for evaluation of pulmonary perfusion. Dual-energy derived iodine maps allow the visualization of parenchymal iodine distribution in relation to a previously defined scan delay, which might be considered as a surrogate of pulmonary perfusion and has shown good correlation compared to nuclear medicine based imaging modalities. However, no prior study correlated the perfusion changes shown in time resolved perfusion imaging modalities such as DCE-MRI to the perfusion changes displayed in DECT-derived iodine maps.

Research frontiers

Time resolved perfusion-imaging modalities such as DCE-MRI and dual-source DECT.

Innovations and breakthroughs

Authors' study shows that perfusion deficits detected on static dual-energy derived iodine maps show a moderate visual correlation with time-resolved DCE-MRI, thus allowing for an assessment of pulmonary perfusion changes as related to a variety of pathology. This is in contrast with prior studies that investigated the role of pulmonary iodine maps to serve as an additional tool providing a functional evaluation of pulmonary perfusion.

Applications

Both, DECT and DCE-MRI should be applied pulmonary embolism imaging. However, the authors think that the results of this study should be viewed as preliminary as only a small number of patients were included and broad inclusion criteria including patients with a variety of underlying pulmonary pathology were applied

Peer review

The authors investigated whether there is correlation between DECT derived iodine maps and parameter maps of quantitative pulmonary perfusion MRI. This is a well-written manuscript, which should be suitable for publication.

REFERENCES

1 **Chiro GD**, Brooks RA, Kessler RM, Johnston GS, Jones AE, Herdt JR, Sheridan WT. Tissue signatures with dual-energy computed tomography. *Radiology* 1979; **131**: 521-523 [PMID: 441344]

2 **Flohr TG**, McCollough CH, Bruder H, Petersilka M, Gruber K, Süss C, Grasruck M, Stierstorfer K, Krauss B, Raupach R, Primak AN, Küttner A, Achenbach S, Becker C, Kopp A, Ohnesorge BM. First performance evaluation of a dual-source CT (DSCT) system. *Eur Radiol* 2006; **16**: 256-268 [PMID: 16341833 DOI: 10.1007/s00330-005-2919-2]

3 **Johnson TR**, Krauss B, Sedlmair M, Grasruck M, Bruder H, Morhard D, Fink C, Weckbach S, Lenhard M, Schmidt B, Flohr T, Reiser MF, Becker CR. Material differentiation by dual energy CT: initial experience. *Eur Radiol* 2007; **17**: 1510-1517 [PMID: 17151859 DOI: 10.1007/s00330-006-0517-6]

4 **Apfaltrer P**, Meyer M, Meier C, Henzler T, Barraza JM, Dint-

er DJ, Hohenberger P, Schoepf UJ, Schoenberg SO, Fink C. Contrast-enhanced dual-energy CT of gastrointestinal stromal tumors: is iodine-related attenuation a potential indicator of tumor response? *Invest Radiol* 2012; **47**: 65-70 [PMID: 21934517 DOI: 10.1097/RLI.0b013e31823003d2]

5 **Ascenti G**, Mazziotti S, Lamberto S, Bottari A, Caloggero S, Racchiusa S, Mileto A, Scribano E. Dual-energy CT for detection of endoleaks after endovascular abdominal aneurysm repair: usefulness of colored iodine overlay. *AJR Am J Roentgenol* 2011; **196**: 1408-1414 [PMID: 21606306 DOI: 10.2214/AJR.10.4505]

6 **Gnannt R**, Fischer M, Goetti R, Karlo C, Leschka S, Alkadhi H. Dual-energy CT for characterization of the incidental adrenal mass: preliminary observations. *AJR Am J Roentgenol* 2012; **198**: 138-144 [PMID: 22194489 DOI: 10.2214/AJR.11.6957]

7 **Guggenberger R**, Gnannt R, Hodler J, Krauss B, Wanner GA, Csuka E, Payne B, Frauenfelder T, Andreisek G, Alkadhi H. Diagnostic performance of dual-energy CT for the detection of traumatic bone marrow lesions in the ankle: comparison with MR imaging. *Radiology* 2012; **264**: 164-173 [PMID: 22570505]

8 **Kim JE**, Lee JM, Baek JH, Han JK, Choi BI. Initial assessment of dual-energy CT in patients with gallstones or bile duct stones: can virtual nonenhanced images replace true nonenhanced images? *AJR Am J Roentgenol* 2012; **198**: 817-824 [PMID: 22451546 DOI: 10.2214/AJR.11.6972]

9 **Thieme SF**, Becker CR, Hacker M, Nikolaou K, Reiser MF, Johnson TR. Dual energy CT for the assessment of lung perfusion--correlation to scintigraphy. *Eur J Radiol* 2008; **68**: 369-374 [PMID: 18775618 DOI: 10.1016/j.ejrad.2008.07.031]

10 **Thieme SF**, Graute V, Nikolaou K, Maxien D, Reiser MF, Hacker M, Johnson TR. Dual Energy CT lung perfusion imaging--correlation with SPECT/CT. *Eur J Radiol* 2012; **81**: 360-365 [PMID: 21185141]

11 **Thieme SF**, Johnson TR, Lee C, McWilliams J, Becker CR, Reiser MF, Nikolaou K. Dual-energy CT for the assessment of contrast material distribution in the pulmonary parenchyma. *AJR Am J Roentgenol* 2009; **193**: 144-149 [PMID: 19542406 DOI: 10.2214/AJR.08.1653]

12 **Nance JW**, Henzler T, Meyer M, Apfaltrer P, Braunagel M, Krissak R, Schoepf UJ, Schoenberg SO, Fink C. Optimization of contrast material delivery for dual-energy computed tomography pulmonary angiography in patients with suspected pulmonary embolism. *Invest Radiol* 2012; **47**: 78-84 [PMID: 21577132]

13 **Hoey ET**, Gopalan D, Screaton NJ. Dual-energy CT pulmonary angiography: A new horizon in the imaging of acute pulmonary thromboembolism. *AJR Am J Roentgenol* 2009; **192**: W341-W32; author reply W343 [PMID: 19457800]

14 **Fink C**, Ley S, Puderbach M, Plathow C, Bock M, Kauczor HU. 3D pulmonary perfusion MRI and MR angiography of pulmonary embolism in pigs after a single injection of a blood pool MR contrast agent. *Eur Radiol* 2004; **14**: 1291-1296 [PMID: 14997336 DOI: 10.1007/s00330-004-2282-8]

15 **Fink C**, Puderbach M, Ley S, Plathow C, Bock M, Zuna I, Kauczor HU. Contrast-enhanced three-dimensional pulmonary perfusion magnetic resonance imaging: intraindividual comparison of 1.0 M gadobutrol and 0.5 M Gd-DTPA at three dose levels. *Invest Radiol* 2004; **39**: 143-148 [PMID: 15076006 DOI: 10.1097/01.rli.0000101482.79137.f4]

16 **Kuder TA**, Risse F, Eichinger M, Ley S, Puderbach M, Kauczor HU, Fink C. New method for 3D parametric visualization of contrast-enhanced pulmonary perfusion MRI data. *Eur Radiol* 2008; **18**: 291-297 [PMID: 17705043 DOI: 10.1007/s00330-007-0742-7]

17 **Nael K**, Fenchel M, Krishnam M, Finn JP, Laub G, Ruehm SG. 3.0 Tesla high spatial resolution contrast-enhanced magnetic resonance angiography (CE-MRA) of the pulmonary circulation: initial experience with a 32-channel phased array coil using a high relaxivity contrast agent. *Invest Radiol* 2007; **42**: 392-398 [PMID: 17507810 DOI: 10.1097/01.rli.0000261937.77365.6a]

18 **Ostergaard L**, Weisskoff RM, Chesler DA, Gyldensted C, Rosen BR. High resolution measurement of cerebral blood flow using intravascular tracer bolus passages. Part I: Mathematical approach and statistical analysis. *Magn Reson Med* 1996; **36:** 715-725 [PMID: 8916022]

19 **Sourbron S,** Dujardin M, Makkat S, Luypaert R. Pixel-by-pixel deconvolution of bolus-tracking data: optimization and implementation. *Phys Med Biol* 2007; **52:** 429-447 [PMID: 17202625]

20 **Sourbron S,** Luypaert R, Morhard D, Seelos K, Reiser M, Peller M. Deconvolution of bolus-tracking data: a comparison of discretization methods. *Phys Med Biol* 2007; **52:** 6761-6778 [PMID: 17975296]

21 **Geyer LL**, Scherr M, Körner M, Wirth S, Deak P, Reiser MF, Linsenmaier U. Imaging of acute pulmonary embolism using a dual energy CT system with rapid kVp switching: initial results. *Eur J Radiol* 2012; **81**: 3711-3718 [PMID: 21420812]

22 **Fink C**, Johnson TR, Michaely HJ, Morhard D, Becker C, Reiser M, Nikolaou K. Dual-energy CT angiography of the lung in patients with suspected pulmonary embolism: initial results. *Rofo* 2008; **180**: 879-883 [PMID: 19238637]

23 **Pontana F**, Faivre JB, Remy-Jardin M, Flohr T, Schmidt B, Tacelli N, Pansini V, Remy J. Lung perfusion with dual-energy multidetector-row CT (MDCT): feasibility for the evaluation of acute pulmonary embolism in 117 consecutive patients. *Acad Radiol* 2008; **15**: 1494-1504 [PMID: 19000866 DOI: 10.1016/j.acra.2008.05.018]

24 **Hoey ET**, Mirsadraee S, Pepke-Zaba J, Jenkins DP, Gopalan D, Screaton NJ. Dual-energy CT angiography for assessment of regional pulmonary perfusion in patients with chronic thromboembolic pulmonary hypertension: initial experience. *AJR Am J Roentgenol* 2011; **196**: 524-532 [PMID: 21343493 DOI: 10.2214/AJR.10.4842]

25 **Fink C**, Risse F, Buhmann R, Ley S, Meyer FJ, Plathow C, Puderbach M, Kauczor HU. Quantitative analysis of pulmonary perfusion using time-resolved parallel 3D MRI - initial results. *Rofo* 2004; **176**: 170-174 [PMID: 14872369 DOI: 10.1055/s-2004-817624]

26 **Ingrisch M**, Dietrich O, Attenberger UI, Nikolaou K, Sourbron S, Reiser MF, Fink C. Quantitative pulmonary perfusion magnetic resonance imaging: influence of temporal resolution and signal-to-noise ratio. *Invest Radiol* 2010; **45**: 7-14 [PMID: 19996761 DOI: 10.1097/RLI.0b013e3181bc2d0c]

P- Reviewer Ma LS **S- Editor** Wen LL
L- Editor A **E- Editor** Xiong L